Scalable two- and four-qubit parity measurement with a threshold photon counter

Luke C. G. Govia,[1,*] Emily J. Pritchett,[1,†] B. L. T. Plourde,[2] Maxim G. Vavilov,[3] R. McDermott,[3] and Frank K. Wilhelm[1]

[1]*Theoretical Physics, Universität des Saarlandes, Campus, 66123 Saarbrücken, Germany*

[2]*Department of Physics, Syracuse University, Syracuse, New York 13244-1130, USA*

[3]*Department of Physics, University of Wisconsin, Madison, Wisconsin 53706, USA*

(Received 11 February 2015; published 14 August 2015)

Parity measurement is a central tool for many quantum information processing tasks. In this work, we propose a method to directly measure two- and four-qubit parity with low overhead in hardware and software while remaining robust to experimental imperfections. Our scheme relies on dispersive qubit-cavity coupling and photon counting that is sensitive only to intensity; both ingredients are widely realized in many different quantum computing modalities. For a leading technology in quantum computing, superconducting integrated circuits, we analyze the measurement contrast and the back action of the scheme and show that this measurement comes close enough to an ideal parity measurement to be applicable to quantum error correction.

DOI: 10.1103/PhysRevA.92.022335 PACS number(s): 03.67.Lx, 03.67.Ac, 42.50.Dv

I. INTRODUCTION

The ability to measure a quantum system in a high-fidelity and quantum nondemolition (QND) way is fundamental to most aspects of quantum information processing (QIP). In the circuit quantum electrodynamics (cQED) community, great success has been achieved in qubit readout by linear amplification and homodyne detection of the signal in a dispersively coupled microwave resonator (cavity) [1–4]. However, the macroscopic size and complicated circuitry required for this readout scheme are a major obstacle to scalability. For this reason a simpler, scalable, high-fidelity, QND single-qubit readout scheme based on threshold photodetection was recently introduced [5].

In addition, QND readout of multiqubit operators is increasingly important in contemporary QIP. In particular, readout of multiqubit parity has applications to quantum error correction [6] such as the surface code [7], quantum phase estimation [8], the implementation of multiqubit gates [9,10], and entanglement generation [11–13]. Parity measurement of two superconducting qubits has been proposed [14] and demonstrated [12,15], as has Bell-state measurement [16] and parity measurement of a cavity state using a superconducting qubit [17]. However, adapting these protocols to more than two qubits requires a significant increase in complexity, either in the number of resonators necessary for amplification-based direct parity measurement [18,19] or in the number of costly entangling gates in gate-based parity measurement.

In this work, we propose a protocol for QND parity readout of multiple qubits coupled to one resonator, over a time scale comparable to that of a single entangling gate. We describe the physical model, briefly review the similar protocol of single-qubit readout [5], present the protocol for N-qubit single-shot parity measurement, and analyze the main sources of error.

We describe parity measurement on N qubits, each coupled to the same single-mode cavity, which is coupled to a tunable photon counter. Each qubit of transition frequency ω_{Q_n} couples to the cavity via a Jaynes-Cummings interaction in the dispersive regime, leading to the cavity-qubit Hamiltonian ($\hbar = 1$)

$$H = H_D + \omega_C \hat{a}^\dagger \hat{a} + \sum_n^N \left(\chi_{Q_n} \hat{a}^\dagger \hat{a} - \frac{\omega_{Q_n} - \chi_{Q_n}}{2} \right) \hat{\sigma}_z^n, \qquad (1)$$

where $\chi_{Q_n} \equiv g_{Q_n}^2/(\omega_C - \omega_{Q_n})$ is the dispersive shift for coupling strength g_{Q_n} and $H_D \equiv A(t)(\hat{a} + \hat{a}^\dagger)$ is a time-dependent classical drive that controls the cavity. For this Hamiltonian the computational basis states are the eigenvectors of $\sum_n^N \hat{\sigma}_z^n$. We assume that the qubits are far enough detuned that cavity-mediated qubit-qubit coupling is negligible. This model is sufficiently general to encompass many qubit architectures [1,3,12,18,20,21].

Our protocol can be applied to any physical system with a threshold photon counter and strong dispersive coupling. In the microwave regime, where photon counting is possible with a Josephson photomultiplier (JPM) [22], other examples include nitrogen-vacancy centers in diamond [23], Rydberg atoms [24,25], and lateral quantum dots [26]. At higher frequencies, where photon counters are commonplace, candidate systems include trapped atoms [27] and self-assembled quantum dots [28].

II. PARITY READOUT PROTOCOL

Described in Ref. [5], cavity-mediated, QND, single-qubit measurement with a photon counter is a three-stage protocol. First the cavity, initialized to vacuum, is driven at its shifted resonance frequency for an excited qubit, populating the cavity conditionally upon the state of the qubit. Next, the photon counter distinguishes between the conditional cavity states (one of which is above and one of which is below its threshold) and therefore detects the state of the qubit. Finally, a microwave drive resets the cavity to the vacuum. Two properties of the counter are crucial: it should be an intensity detector that responds to the total energy only (insensitive to phase), and it should have threshold behavior at a photon number that is well between vacuum and the selectively excited state of the

*lcggovia@lusi.uni-sb.de

†Present address: HRL Laboratories, LLC, Malibu, California 90265, USA.

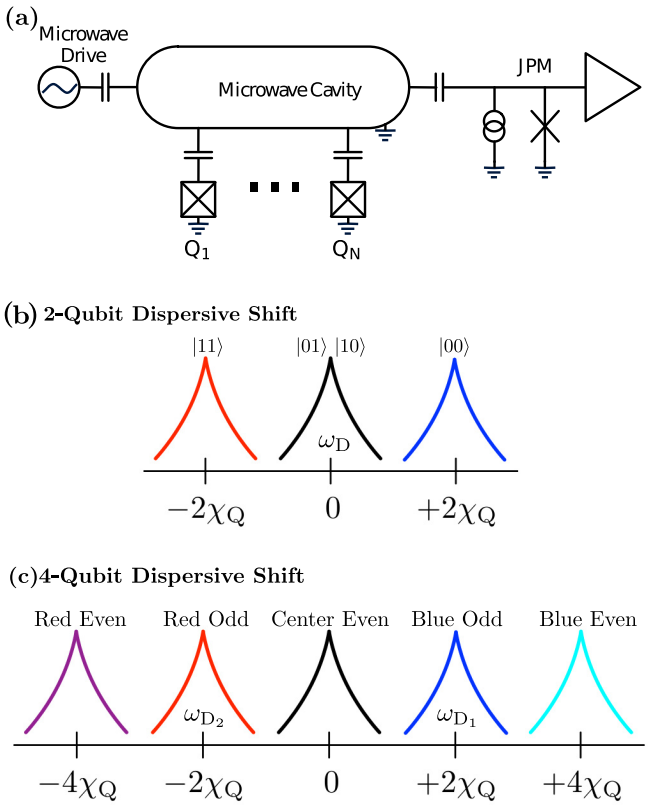

FIG. 1. (Color online) (a) Schematic of the experimental design showing the cavity, N coupled qubits, and the photon counter (a JPM in this case). (b) and (c) Illustration of the dispersive shifts on the cavity for two- and four-qubit computational basis states.

cavity. Number resolution and single-photon sensitivity are *not* required.

During the drive stage, the reduced Hamiltonian of the cavity coupled to a single qubit,

$$\hat{H}_{\mathrm{C}} = \tilde{\omega}_{\mathrm{C}}\hat{a}^{\dagger}\hat{a} + A(t)(\hat{a} + \hat{a}^{\dagger}), \tag{2}$$

is that of a single-mode oscillator with resonance frequency $\tilde{\omega}_{\mathrm{C}} = \omega_{\mathrm{C}} + \tilde{\chi}_{\mathrm{Q}}$, where $\tilde{\chi}_{\mathrm{Q}} = s\chi_{\mathrm{Q}}$ encodes the state of the qubit through $s = \pm 1$, with s being the respective eigenvalue of $\hat{\sigma}_z$. By a carefully timed classical drive at frequency $\omega_{\mathrm{D}} = \omega_{\mathrm{C}} - \chi_{\mathrm{Q}}$, we put the cavity in a high-amplitude coherent state if the qubit is excited but in the vacuum state if the qubit is in its ground state, thus dephasing the qubit. The cavity is populated conditionally upon the qubit having odd parity (excited state), via the unitary

$$\hat{U}_{\mathrm{D}} = \hat{P}_{\mathrm{Q}}^{\mathrm{E}} \otimes \mathbb{I}_{\mathrm{C}} + \hat{P}_{\mathrm{Q}}^{\mathrm{O}} \otimes \hat{D}(\beta), \tag{3}$$

where $\hat{D}(\beta)$ is the displacement operator. Here $\hat{P}_{\mathrm{Q}}^{\mathrm{E}}$ and $\hat{P}_{\mathrm{Q}}^{\mathrm{O}}$ are projectors onto the even- and odd-parity subspaces, which are projectors onto the ground and excited states for single-qubit readout, while for $N > 1$ they are sums of projectors onto a set of states spanning each parity subspace. This is a quantum eraser that transfers parity information to the cavity amplitude and all other qubit-state information to the phase.

Now consider two qubits coupled to the cavity with equal dispersive shifts. For the computational basis states the total dispersive shift on the cavity is $\tilde{\chi}_{\mathrm{Q}} = \pm 2\chi_{\mathrm{Q}}$ when both qubits are in the same eigenstate (even parity) and $\tilde{\chi}_{\mathrm{Q}} = 0$ when the qubits are in different eigenstates (odd parity), as illustrated in Fig. 1(b). By driving with frequency $\omega_{\mathrm{D}} = \omega_{\mathrm{C}}$ we entangle the qubit parity subspaces with distinguishable cavity states, implementing the unitary of Eq. (A12). At the end of the drive pulse $A(t) = a_0 \cos(\omega_{\mathrm{D}} t + \phi)\Theta(t_{\mathrm{D}} - t)$, the qubit-dependent cavity occupations are

$$|\alpha_{\mathrm{E}}|^2 = \left(\frac{a_0}{\Delta_{\mathrm{D}}}\right)^2 \frac{1 - \cos(\Delta_{\mathrm{D}} t_{\mathrm{D}})}{2}, \quad |\alpha_{\mathrm{O}}|^2 = \left(\frac{a_0}{2} t_{\mathrm{D}}\right)^2,$$

where $\Delta_{\mathrm{D}} = \tilde{\omega}_{\mathrm{C}} - \omega_{\mathrm{D}}$. Setting $\omega_{\mathrm{D}} = \omega_{\mathrm{C}}$ gives $|\Delta_{\mathrm{D}}| = 2\chi_{\mathrm{Q}}$ for even-parity states, and therefore, $|\alpha_{\mathrm{E}}|^2 = 0$ at $t_{\mathrm{D}} = \pi/\chi_{\mathrm{Q}}$ ($\Delta_{\mathrm{D}} = 0$ for the odd states). As $\alpha_{\mathrm{E}} = 0$, the even-parity states are indistinguishable, and all state information other than parity has been erased. Thus, while coherence between subspaces with different parities is reduced to $\langle\alpha_{\mathrm{O}}|\alpha_{\mathrm{E}}\rangle$, intrasubspace coherence is protected, unlike in direct parity measurement [12].

For $N > 2$ qubits, the degeneracy within the odd and even subspaces splits, and we cannot perform parity measurement by a single-frequency cavity drive. However, with

$$A(t) = a_0 \sum_i \cos\left(\omega_{\mathrm{D}_i} t + \phi\right) \quad 0 \leqslant t \leqslant t_{\mathrm{D}}, \tag{4}$$

where $\omega_{\mathrm{D}_i} = \omega_{\mathrm{C}} + \tilde{\chi}_{\mathrm{Q}_i}$ are the dispersively shifted cavity frequencies for each band of the odd-parity subspace, we apply the unitary of Eq. (A12) by simultaneously driving all odd-parity spectral lines resonantly with a multitone drive (see Appendix A for further details). Here multiplexing is used to measure a binary observable, extracting less qubit information than full multiplexed readout [29,30], at a reduced cost in complexity.

For four qubits, odd-parity basis states produce dispersive shifts of $\pm 2\chi_{\mathrm{Q}}$ (blue and red odd-parity bands), while even-parity basis states cause shifts of 0 or $\pm 4\chi_{\mathrm{Q}}$, as shown in Fig. 1(c). Therefore, with two drive frequencies $\omega_{\mathrm{D}_{1,2}} = \omega_{\mathrm{C}} \pm 2\chi_{\mathrm{Q}}$ we simultaneously drive both odd-parity spectral lines. The cavity occupations for the four-qubit parity bands are shown in Fig. 2 (see Appendix A for their analytic form). Crucially, $|\alpha_{\mathrm{E}}|^2 = 0$ for all even-parity states at $t_{\mathrm{D}} = \pi/\chi_{\mathrm{Q}}$, while $|\alpha_{\mathrm{O}}|^2$ are equal for all odd-parity states. Therefore, qubit

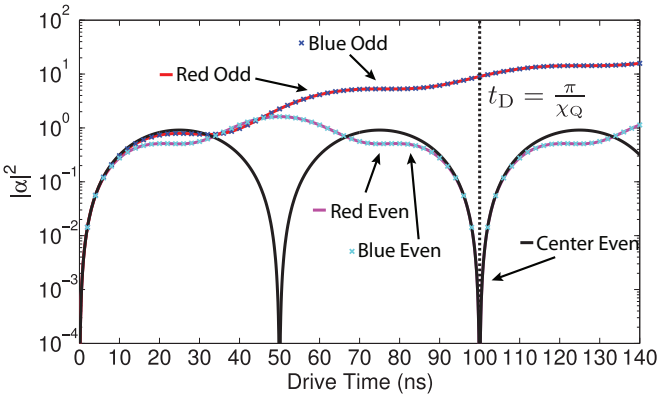

FIG. 2. (Color online) Cavity photon number as a function of the length of the drive pulse t_{D} for the four-qubit parity bands. $\chi_{\mathrm{Q}}/\pi = 10$ MHz, so the optimal drive time is $t_{\mathrm{D}} = 100$ ns, which for $|\alpha_{\mathrm{O}}|^2 = 9$ sets $a_0 = 0.06$ MHz.

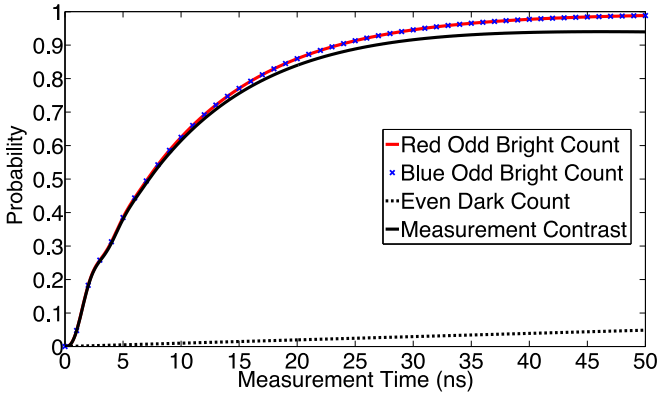

FIG. 3. (Color online) Bright-count probability for the four-qubit odd-parity bands, dark-count probability for even parity, and measurement contrast as functions of measurement time. The JPM bright count rate, inelastic relaxation rate, and dark-count rate are $\gamma_J = 200$ MHz, $\gamma_R = 200$ MHz, and $\gamma_D = 1$ MHz. The cavity-JPM coupling is $g_J/2\pi = 50$ MHz.

parity information has been mapped onto cavity occupation in a way that erases all other qubit-state information.

In the measurement stage we distinguish between the qubit-parity-dependent cavity states in a frequency- and phase-insensitive way (to avoid intrasubspace decoherence) by using a high-bandwidth photon counter. We tune the counter on resonance with the bare cavity frequency ω_C. For two qubits, the counter and cavity are resonant for odd-parity qubit states, maximizing the detection probability of $|\alpha_O\rangle$. For four qubits, the counter is resonant with the cavity if the qubits are in the center even-parity band; however, this is not an issue because the cavity is unoccupied for even-parity qubits. The counter will be $\pm 2\chi_Q$ off resonance from the cavity for odd-parity qubits, symmetrically between the two odd-parity cavity frequencies. For a counter with bandwidth $>4\chi_Q$ this ensures the detection probabilities for all odd-parity states are identical, minimizing intrasubspace decoherence.

For $N = 4$, the bright-count detection probability for the two odd-parity bands is shown in Fig. 3, as is the false "even-state detection probability" due to dark counts. As expected, the two bright-count curves are identical. These curves are calculated by solving the master equation with relevant experimental parameters (for further information see Appendix B). As an example of a threshold photon counter we have chosen the JPM, which, coupled to a cavity, approaches unit detection probability with large bandwidth ($\gg\chi_Q$) [31,32]. Recent progress has been made with a JPM coupled to a cavity-qubit system with initial steps towards single-qubit readout [33]. We note that similar detectors exist in the optical [34,35] and near-infrared [36] regimes.

As a figure of merit we consider the parity measurement contrast, defined as

$$C(t_M) \equiv P(|\alpha_O|^2, t_M) - P(|\alpha_E|^2, t_M), \tag{5}$$

the difference in detection probability between odd and even parity states, which is a function of measurement time t_M. The drive time t_D is chosen such that $\alpha_E = 0$, so the parity measurement contrast reduces to the bright-count probability minus the dark-count probability. In reality there will be thermal photons in the cavity. However, because of the threshold nature of the photon counter an initially empty cavity is not necessary to maximize measurement contrast; it is sufficient that the detection probability has a sharp threshold between α_O and α_E. This is important for the JPM, where the threshold can be set at zero occupation in principle [31,32], however, this can be often difficult to engineer. Nonetheless, a suitable threshold between α_O and α_E is easily obtained [5].

Parity measurement contrast is limited by misidentification of the parity, which occurs either due to a dark count or the nonzero probability of not detecting the state $|\alpha_O\rangle$. These errors are controlled by the bright-to-dark-count ratio of the photon counter and the cavity occupation $|\alpha_O|^2$, and control over these parameters is sufficient to obtain contrast arbitrarily close to unity. As seen in Fig. 3, measurement contrast that approaches 95% is achievable, compatible with the readout threshold for error correction [7,37], in a 40-ns time frame with experimentally relevant bright-to-dark-count ratio and $|\alpha_O|^2$.

In the reset stage we implement the qubit-dependent cavity displacement of Eq. (A12), but with $\beta = -\alpha_M$. For odd-parity states, the cavity begins approximately in the coherent state $|\alpha_M\rangle$ and is returned to vacuum, where $|\alpha_M|$ is calculated given the input magnitude $|\alpha_O|$ and the form of the detection back action on the cavity [38]. For a JPM, after measurement the cavity is not a coherent state, and reset is imperfect. However, single-shot parity measurement is unaffected by reset error, and although repeated measurements are affected, for experimentally relevant parameters reset error is on the order of 1% [5].

III. ERROR ANALYSIS AND PROTOCOL COMPARISONS

In a realistic experiment it is unlikely that all qubit-cavity dispersive shifts will be identical. Therefore, we examine the robustness of our protocol against variations in the dispersive shifts, defining the dispersive shift error ϵ, such that $\chi_{Q_1} = \chi_Q$ and $\chi_{Q_2} = \chi_Q + \epsilon$ for two qubits. For four qubits there are three dispersive shift errors: ϵ_2, ϵ_3, and ϵ_4. We assume this error is small, such that $\epsilon_i/\chi_Q \ll 1$. For a superconducting qubit with coherence time 5 μs, the uncertainty in χ_Q due to homogeneous broadening is no more than $\pm 0.1\%$, and thus, $|\epsilon_i/\chi_Q| < 0.2\%$. Mismatch in χ_Q causes a reduction in measurement contrast and intrasubspace decoherence (dephasing of a superposition of qubit states of the same parity). We provide quantitative estimates of these effects, leaving further details to Appendices C and D. Errors in the drive frequencies ω_{D_i} cause errors similar to those for χ_Q mismatch but can be corrected for during tune-up.

Imperfect resonance between the applied drives and the cavity due to χ_Q mismatch leads to a reduced $|\alpha_O|^2$ and increased $|\alpha_E|^2$. The reduction in measurement contrast due to this is second order in ϵ_i/χ_Q, commensurate with a square-law detector. As shown in Fig. 4, even for 10% χ_Q mismatch, the resulting measurement error (even-state detection probability) is on the order of 1%.

The intrasubspace decoherence caused by χ_Q mismatch is due to qubit states with the same parity being entangled to cavity states with different phases, which are distinguishable in principle. The resulting decoherence is at most second order in ϵ_i/χ_Q. Shown in Fig. 4 is the coherence of odd- and

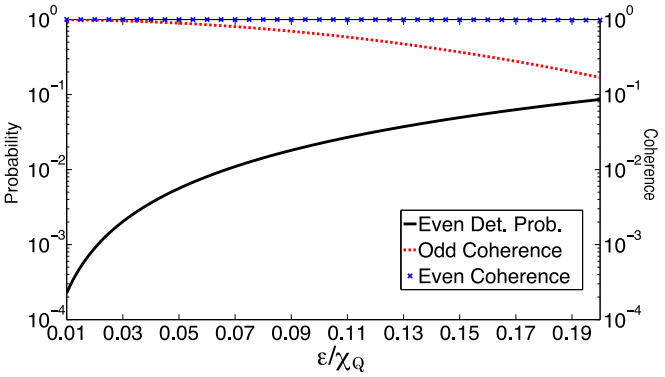

FIG. 4. (Color online) Even-parity detection probability, odd-parity coherence, and even-parity coherence as functions of the χ_Q mismatch for two-qubit parity measurement. ϵ/χ_Q ranges from 1% to 20%, well within experimental expectations. $\chi_Q/2\pi = 5$ MHz, and the drive power a_0 is such that $|\alpha_O|^2 = 9$.

even-parity two-qubit superposition states, quantified by the relevant off-diagonal matrix element of the reduced two-qubit density matrix. Although the decoherence of an odd-parity superposition is nontrivial for larger values of ϵ/χ_Q, perfect reset returns full coherence by depopulating the cavity in a phase-insensitive way.

However, any cavity decay prior to perfect reset will cause irreversible decoherence, as would the decay of residual photons after imperfect reset. Up to the limit of strong χ_Q mismatch (ϵ approaching χ_Q), the intrasubspace coherence decays to $\exp\{-N_C[1-\cos(\pi\epsilon/\chi_Q)]\}$ in the steady state, where N_C is the average photon number in the cavity prior to decay, hence requiring $\epsilon < \chi_Q/\sqrt{N_C}$. For a high-$Q$ cavity, decay during the short measurement time is unlikely, and postreset cavity decay is the significant source of loss. For the parameters considered here, the residual photons after imperfect reset result in coherence loss less than 1% in the worst case, which is inconsequential.

For two qubits with χ_Q mismatch, no intrasubspace decoherence occurs during the measurement stage as cavity states corresponding to qubit states of the same parity have equal detection probability. For four qubits the detection probabilities of cavity states within the same parity subspace can be different, with their difference scaling as $(\epsilon_i^2 - \epsilon_j^2)/\chi_Q^2$. This changes the basis of measurement, changing the qubit state at the protocol's end. This effect can be mitigated by a square-law photon counter that quickly saturates with photon number once above threshold, such as the JPM, for which the error in the output qubit state is negligible.

Higher-order effects beyond the dispersive Hamiltonian can affect the parity readout protocol presented here. As a result of the formation of cavity-qubit dressed states, there is residual cavity occupation for even-parity states, which reduces parity measurement contrast. For four qubits the contrast is reduced to ≈92% (see Appendix E). However, contrast can be improved by increasing cavity-qubit detuning and/or using better drive pulse sequences. The protocol's QND character will also be affected by higher-order terms; however, as shown for single-qubit readout in [5], this effect is minimal. As the measurement stages of single-qubit readout and parity readout are very similar, this is also true for parity readout.

Our protocol involves an entangling operation that maps qubit information to the cavity such that destructive readout of the cavity nondestructively determines the qubits' parity. It provides a tailored and efficient quantum circuit that maps parity information onto an ancilla (the cavity) and measures the ancilla in a way that is insensitive to qubit-resolving information. It occupies a middle ground between direct parity measurement [14,18,19] and gate-based parity measurement. The advantage of our protocol over gate-based protocols is the reduced number of entangling gates required: one for our proposal *versus* N for the gate-based N-qubit protocol. This allows for readout fidelity that is not bounded by gate fidelity. Our protocol also requires fewer cavities than direct four-qubit parity readout [18,19] and avoids the intrasubspace decoherence often introduced by these protocols.

IV. CONCLUSION

In conclusion we have presented a high-fidelity, scalable, QND protocol for parity readout of two or four qubits via photon counting of a dispersively coupled cavity. Measurement contrast is limited by the bright-to-dark-count ratio of the counter and, with the limited optimization in this work, approaches 95%. Our protocol introduces no decoherence of qubit states with the same parity and is robust against major sources or error. Future work will focus on protocol optimization and higher-order corrections.

ACKNOWLEDGMENTS

This work was supported by the Army Research Office under Contract No. W911NF-14-1-0080. L.C.G.G., E.J.P., and F.K.W. also acknowledge support from the European Union through ScaleQIT, and L.C.G.G. acknowledges support from NSERC through an NSERC PGS-D. M.G.V., and R.M. were also supported by NSF Grant No. DMR-1105178.

APPENDIX A: DERIVATION OF THE QUBIT-PARITY-DEPENDENT DRIVE FOR FOUR QUBITS

In this Appendix we derive the driven cavity evolution for four qubits, as shown in Fig. 2 of the main text. The full system Hamiltonian is block diagonal, with one block for each state of the qubits. In each block the effective cavity Hamiltonian is

$$\hat{H}_C = \tilde{\omega}_C \hat{a}^\dagger \hat{a} + a_0\big[\cos\left(\omega_{D_1} t + \phi_1\right) + \cos\left(\omega_{D_2} t + \phi_2\right)\big]\Theta(t_D - t)(\hat{a} + \hat{a}^\dagger), \quad \text{(A1)}$$

where the shifted cavity frequency $\tilde{\omega}_C = \omega_C + \tilde{\chi}_Q$ depends on the qubit-state dependent dispersive shift $\tilde{\chi}_Q = \chi_Q\langle\hat{\sigma}_z\rangle$, which defines the state of the qubits and therefore the corresponding block of the full Hamiltonian. $\tilde{\chi}_Q = \pm 2\chi_Q$ for odd-parity states, and $\tilde{\chi}_Q = 0, \pm 4\chi_Q$ for even parity.

We go to a frame rotating with the shifted cavity frequency $\tilde{\omega}_C$ to obtain

$$\hat{H}'_C = \frac{a_0}{2}\Theta(t_D - t)[\hat{a}(e^{-i\Delta_1 t} + e^{-i\Delta_2 t}) + \text{h.c.}], \quad \text{(A2)}$$

where $\Delta_i = \tilde{\omega}_C - \omega_{D_i}$. We formally solve for the evolution operator in each block for times $t \geqslant t_D$ as

$$\hat{U}(t,0) = \mathcal{T}\exp\left\{-i\int_0^{t_D} \hat{H}'_C(t')dt'\right\}, \tag{A3}$$

where $\mathcal{T}$ is the time-ordering operator. The evolution operator for the full system then has the form

$$\hat{U}_D = \sum_j |j\rangle\langle j| \otimes \hat{U}_j(t,0), \tag{A4}$$

where $\hat{U}_j(t,0)$ are the solutions to Eq. (A3) for each qubit state $|j\rangle$ in the computational basis.

We evaluate the integral in Eq. (A3) using the Magnus expansion [39] to take care of the time ordering. Because $[\hat{a},\hat{a}^\dagger] = 1$, the Magnus expansion truncates at second order, and conveniently, the second-order term is a global phase that we can ignore. We evaluate the integral in two regimes, corresponding to even or odd parity, and in so doing obtain the solution for the blocks of the full Hamiltonian. For even parity, $\Delta_1 \neq 0$ and $\Delta_2 \neq 0$, and to first order we have

$$\int_0^{t_D} \hat{H}'_C(t')dt' = \frac{a_0}{2}\left\{\hat{a}\left[\frac{i}{\Delta_1}(e^{-i\Delta_1 t_D} - 1) + \frac{i}{\Delta_2}(e^{-i\Delta_2 t_D} - 1)\right] + \text{h.c.}\right\}.$$

The evolution operator of Eq. (A3) for even parity is then

$$\hat{U}_E(t,0) = \hat{D}(\alpha_E(t_D)), \tag{A5}$$

where

$$\alpha_E(t_D) = -\frac{a_0}{2}\left[\frac{e^{i\Delta_1 t_D} - 1}{\Delta_1} + \frac{e^{i\Delta_2 t_D} - 1}{\Delta_2}\right]. \tag{A6}$$

In general $\alpha_E(t_D)$ varies in phase for different even-parity qubit states as $\Delta_{1,2}$ depend on the specific state.

For an odd-parity qubit basis state, the shifted cavity will be on resonant with one of the two applied drives, and therefore, one Δ_i is zero, while the other is nonzero. Since the solution is symmetric in regards to which $\Delta_i = 0$, we will examine $\Delta_1 = 0$ and $\Delta_2 \neq 0$ without loss of generality. The integral in Eq. (A3) now gives

$$\int_0^{t_D} \hat{H}'_C(t')dt' = \frac{a_0}{2}\left[\hat{a}\left(t_D + i\frac{e^{-i\Delta_2 t_D} - 1}{\Delta_2}\right) + \text{h.c.}\right],$$

which leads to the odd-parity evolution operator

$$\hat{U}_O(t,0) = \hat{D}(\alpha_O(t_D)) = \hat{D}(\beta(t_D) + \eta(t_D)), \tag{A7}$$

where

$$\beta(t_D) = -\frac{ia_0}{2}t_D, \tag{A8}$$

$$\eta(t_D) = -\frac{a_0}{2\Delta_2}(e^{i\Delta_2 t_D} - 1). \tag{A9}$$

In this case it is important to note that while $\eta(t_D)$ varies between odd-parity states, $\beta(t_D)$ is the same for all odd-parity states.

If $\omega_{D_1} = 2\chi_Q$ and $\omega_{D_2} = -2\chi_Q$ as in the main text, then for even parity we have $\Delta_1, \Delta_2 \in \{\pm 2\chi_Q, \pm 6\chi_Q\}$. For odd parity, we have chosen $\Delta_1 = 0$, which means that $\Delta_2 = 4\chi_Q$. Thus, if we set $t_D = \pi/\chi_Q$, we have that $\alpha_E(t_D) = 0$ and $\eta(t_D) = 0$, while $\beta(t_D) \neq 0$. As a result of this,

$$\hat{U}_E(t,0) = \hat{D}(0) = \mathbb{I}, \tag{A10}$$

$$\hat{U}_O(t,0) = \hat{D}(\beta(t_D)), \tag{A11}$$

and the evolution operators are the same for all states within the same parity subspace. This, along with the block-diagonal form of the full system Hamiltonian, implies that the unitary on the full system will have the form

$$\hat{U}_D = \sum_{j\in\text{even}} |j\rangle\langle j| \otimes \hat{U}_E(t,0) + \sum_{j\in\text{odd}} |j\rangle\langle j| \otimes \hat{U}_O(t,0) = \hat{P}_Q^E \otimes \mathbb{I}_C + \hat{P}_Q^O \otimes \hat{D}(\beta), \tag{A12}$$

where $\hat{P}_Q^{E,O}$ are projectors onto the even- and odd-parity subspaces, respectively.

APPENDIX B: MASTER EQUATION FOR THE CAVITY-JPM COUPLED SYSTEM

In this Appendix we describe the methodology of the numerical simulations used to obtain Fig. 3 of the main text, which shows the detection probability and parity contrast for our example threshold detector, the JPM.

We start with the cavity-JPM coupled system for four-qubit odd parity, where the shifted cavity frequencies $\tilde{\omega}_C = \omega_C \pm 2\chi_Q$ and the JPM frequency $\omega_J = \omega_C$ are such that the JPM is $\pm 2\chi_Q$ detuned from the cavity. This leads to the Hamiltonian

$$\hat{H}_{JC} = \tilde{\omega}_C \hat{a}^\dagger\hat{a} - \frac{\omega_J}{2}\hat{\sigma}_J + g_J(\hat{a}\hat{\sigma}_J^+ + \hat{a}^\dagger\hat{\sigma}_J^-),$$

where $\hat{\sigma}_J^\pm$ couple the ground and excited states of the JPM. As shown previously [22,31,32,40], the JPM is well approximated as a three-level system with self-Hamiltonian $H_J = -\frac{\omega_J}{2}\sigma_J$, where $\hat{\sigma}_J \equiv \text{diag}(1,-1,k)$. The energy of the third "measurement" state is arbitrary in our model; the JPM only tunnels into it incoherently at fixed rates [31,32].

In addition, the JPM experiences a number of incoherent processes. Tunneling from the JPM excited state to the measured state corresponds to photon detection and occurs at the bright-count rate γ_J, with the corresponding Lindblad operator

$$\hat{L}_2 = \sqrt{\gamma_J}(\mathbb{I}_C \otimes |m\rangle\langle 1|_J). \tag{B1}$$

Inelastic relaxation takes the JPM from the excited state to the ground state at a rate γ_R, with corresponding Lindblad operator

$$\hat{L}_1 = \sqrt{\gamma_R}(\mathbb{I}_C \otimes |0\rangle\langle 1|_J). \tag{B2}$$

Finally, false detections, where the JPM tunnels from the ground state to the measured state, can occur at the dark-count rate γ_D, with Lindblad operator

$$\hat{L}_0 = \sqrt{\gamma_D}(\mathbb{I}_C \otimes |m\rangle\langle 0|_J). \tag{B3}$$

We ignore the effects of pure dephasing on the JPM as they do not affect the parity measurement protocol of the main text.

We solve the master equation

$$\dot{\rho}(t) = -i[\hat{H}_{\rm JC}, \rho(t)] + \sum_{\mu=0}^{2}\left(\hat{L}_\mu \rho(t)\hat{L}_\mu^\dagger - \frac{1}{2}\{\hat{L}_\mu^\dagger \hat{L}_\mu, \rho(t)\}\right), \tag{B4}$$

with $\gamma_{\rm J} = 200$ MHz, $\gamma_{\rm R} = 200$ MHz, $\gamma_{\rm D} = 1$ MHz, and $g_{\rm J}/2\pi = 50$ MHz for both $\tilde{\omega}_{\rm C} - \omega_{\rm C} = 2\chi_{\rm Q}$ and $-2\chi_{\rm Q}$ (where $\chi_{\rm Q}/2\pi = 5$ MHz) to generate the detection probability curves of Fig. 3.

APPENDIX C: QUBIT DISPERSIVE SHIFT MISMATCH

In this Appendix we examine in detail the possible sources of error caused by $\chi_{\rm Q}$ mismatch that were described in the main text and shown in Fig. 4. First, we quantify the decrease in measurement contrast and the coherence loss for two qubits. As described in the main text, this coherence loss can be restored by perfect reset. We then examine these effects for four qubits and also quantify the change in the measurement basis due to detection probability mismatch, which is unique to four qubits.

1. Two qubits

If the dispersive shifts for the two qubits vary, such that $\chi_{\rm Q_1} = \chi_{\rm Q}$ and $\chi_{\rm Q_2} = \chi_{\rm Q} + \epsilon$, then the cavity-drive detunings within a parity subspace split, such that we now have

$$\begin{aligned}\Delta_{00} &= -2\chi_{\rm Q} - \epsilon,\\ \Delta_{11} &= 2\chi_{\rm Q} + \epsilon,\\ \Delta_{01} &= \epsilon,\\ \Delta_{10} &= -\epsilon,\end{aligned} \tag{C1}$$

where Δ_{ij} is the cavity-drive detuning for the state $|ij\rangle$.

After a time $t_{\rm D} = \pi/\chi_{\rm Q}$ the cavity will be in a qubit-state-dependent coherent state with amplitude

$$\begin{aligned}\alpha_{00} &= \frac{a_0}{2(2\chi_{\rm Q}+\epsilon)}\left(e^{-i\frac{\pi}{\chi_{\rm Q}}\epsilon} - 1\right),\\ \alpha_{11} &= -\frac{a_0}{2(2\chi_{\rm Q}+\epsilon)}\left(e^{i\frac{\pi}{\chi_{\rm Q}}\epsilon} - 1\right),\\ \alpha_{01} &= -\frac{a_0}{2\epsilon}\left(e^{i\frac{\pi}{\chi_{\rm Q}}\epsilon} - 1\right),\\ \alpha_{10} &= \frac{a_0}{2\epsilon}\left(e^{-i\frac{\pi}{\chi_{\rm Q}}\epsilon} - 1\right).\end{aligned} \tag{C2}$$

For the even-parity qubit states we have $\alpha_{11} = -\bar{\alpha}_{00}$, and for the odd-parity states $\alpha_{10} = -\bar{\alpha}_{01}$. As a result, states within the same parity subspace will have the same detection probability, so there will be no intrasubspace decoherence during the measurement stage. However, as $|\alpha_{00}| \neq 0$, there will be a reduction of measurement contrast due to the increased probability of misidentification. As the coherent states for each parity subspace are out of phase with one another, there also will be intrasubspace decoherence during the drive stage. We will now quantify these effects in the $\epsilon/\chi_{\rm Q} < 1$ regime.

For the measurement contrast and misidentification we can quantify the effect of $\chi_{\rm Q}$ mismatch by looking at the cavity occupation for odd parity, $|\alpha_{\rm O}|^2 = |\alpha_{01}|^2 = |\alpha_{10}|^2$, and for even parity, $|\alpha_{\rm E}|^2 = |\alpha_{00}|^2 = |\alpha_{11}|^2$. For odd parity

$$\begin{aligned}|\alpha_{\rm O}|^2 &= \left(\frac{a_0}{2\epsilon}\right)^2\left[2 - 2\cos\left(\frac{\pi\epsilon}{\chi_{\rm Q}}\right)\right]\\ &= \left(\frac{a_0}{2}\right)^2\left(\frac{\pi}{\chi_{\rm Q}}\right)^2\left[1 - \frac{1}{12}\left(\frac{\pi\epsilon}{\chi_{\rm Q}}\right)^2\right] + O(\varepsilon^4),\end{aligned} \tag{C3}$$

where $\varepsilon = \epsilon/\chi_{\rm Q}$, and we see that the reduction of $|\alpha_{\rm O}|^2$ from that when the dispersive shifts are perfectly matched is second order in $\epsilon/\chi_{\rm Q}$. Similarly, for even parity

$$\begin{aligned}|\alpha_{\rm E}|^2 &= \left(\frac{a_0}{2(2\chi_{\rm Q}+\epsilon)}\right)^2\left[2 - 2\cos\left(\frac{\pi\epsilon}{\chi_{\rm Q}}\right)\right]\\ &= \left(\frac{a_0}{2(2\chi_{\rm Q}+\epsilon)}\right)^2\left(\frac{\pi\epsilon}{\chi_{\rm Q}}\right)^2 + O(\varepsilon^4)\\ &= \left(\frac{a_0}{2}\right)^2\left(\frac{\pi}{\chi_{\rm Q}}\right)^2\left(\frac{\epsilon}{2\chi_{\rm Q}}\right)^2 + O(\varepsilon^4),\end{aligned} \tag{C4}$$

and the increase in $|\alpha_{\rm E}|^2$ from that when the dispersive shifts are perfectly matched is again second order in $\epsilon/\chi_{\rm Q}$. The fact that the lowest-order dependence is quadratic originates from the expansion of the cosine and can be physically explained by the fact that the amplitude is originally tuned to zero, and a square-law detector responds to intensity which is $|\alpha|^2$.

To quantify the intrasubspace decoherence during the drive stage, we consider an arbitrary superposition of odd-parity states with the cavity initially in vacuum, to which we apply the modified qubit-state-dependent drive (accounting for $\chi_{\rm Q}$ mismatch). The resulting state

$$|\Psi\rangle = a|01\rangle|\alpha_{01}\rangle + b|10\rangle|\alpha_{10}\rangle, \tag{C5}$$

where $|a|^2 + |b|^2 = 1$, is no longer a product state, and as such there will necessarily be decoherence of the reduced qubit state. The reduced qubit state is

$$\rho_{\rm Q} = \begin{pmatrix} 0 & 0 & 0 & 0\\ 0 & |a|^2 & \bar{D}a\bar{b} & 0\\ 0 & D\bar{a}b & |b|^2 & 0\\ 0 & 0 & 0 & 0\end{pmatrix}, \tag{C6}$$

with the complex decoherence factor

$$D = \langle\alpha_{01}|\alpha_{10}\rangle = \exp\left\{-\left(|\alpha_{01}|^2 + \bar{\alpha}_{01}^2\right)\right\}. \tag{C7}$$

From Eq. (C2) we see that

$$|\alpha_{01}|^2 = 2A_{\rm O}^2\left[1 - \cos\left(\frac{\pi\epsilon}{\chi_{\rm Q}}\right)\right], \tag{C8}$$

$$\bar{\alpha}_{01}^2 = A_{\rm O}^2\left\{1 - 2\left[\cos\left(\frac{\pi\epsilon}{\chi_{\rm Q}}\right) - i\sin\left(\frac{\pi\epsilon}{\chi_{\rm Q}}\right)\right] + \cos\left(2\frac{\pi\epsilon}{\chi_{\rm Q}}\right) - i\sin\left(2\frac{\pi\epsilon}{\chi_{\rm Q}}\right)\right\}, \tag{C9}$$

where $A_{\rm O} = a_0/2\epsilon$.

Keeping only the first nonzero term in the Taylor series expansion, we find

$$|\alpha_{01}|^2+\bar{\alpha}_{01}^2 = A_{\rm O}^2\left[\frac{1}{2}\left(\frac{\pi\epsilon}{\chi_{\rm Q}}\right)^4+i\left(\frac{\pi\epsilon}{\chi_{\rm Q}}\right)^3\right] = \left(\frac{a_0}{2}\right)^2\left(\frac{\pi}{\chi_{\rm Q}}\right)^2\left[\frac{1}{2}\left(\frac{\pi\epsilon}{\chi_{\rm Q}}\right)^2+i\frac{\pi\epsilon}{\chi_{\rm Q}}\right]+O(\varepsilon^3). \tag{C10}$$

As can be seen, for an odd-parity superposition, $\chi_{\rm Q}$ mismatch causes decoherence at a rate that is second order in the small parameter ϵ/χ and also introduces a complex phase factor that is first order in ϵ/χ.

For an even-parity superposition, we simply replace $A_{\rm O}$ with the corresponding expression for even states, and we find

$$|\alpha_{00}|^2+\bar{\alpha}_{00}^2 = \left(\frac{a_0}{2(2\chi_{\rm Q}+\epsilon)}\right)^2\left[\frac{1}{2}\left(\frac{\pi\epsilon}{\chi_{\rm Q}}\right)^4+i\left(\frac{\pi\epsilon}{\chi_{\rm Q}}\right)^3\right] = \left(\frac{a_0}{4\chi_{\rm Q}}\right)^2\left[\frac{1}{2}\left(\frac{\pi\epsilon}{\chi_{\rm Q}}\right)^4+i\left(\frac{\pi\epsilon}{\chi_{\rm Q}}\right)^3\right]+O(\varepsilon^5). \tag{C11}$$

Thus, the even-parity situation is even better, as the decoherence rate is now fourth order in ϵ/χ and the complex phase factor is now third order.

For both odd- and even-parity superpositions full intrsubspace coherence will be returned to the two qubits by perfect reset, as it disentangles the qubits and the cavity in a unitary and phase-insensitive way. However, if cavity decay occurs before reset or imperfect reset leaves residual photons which subsequently decay, the qubit state will lose coherence, as will be discussed in Appendix D.

2. Four qubits

The situation is considerably more complex in the four-qubit case as the cavity-drive detunings split into 16 distinct frequencies, one for each qubit state. Correspondingly, after the qubit-state-dependent drive there are 16 possible cavity states $|\alpha_{ijkl}\rangle$, where $i,j,k,l\in\{0,1\}$ index the qubit state $|ijkl\rangle$. As a result of the double-frequency drive each α_{ijkl} will have two components oscillating at different frequencies, with each component similar in form to those of Eq. (C2). Cavity states for even qubit parity will have both components of the form of α_{00}, where the amplitude is suppressed by a factor $1/(2\chi_{\rm Q}+\epsilon)$, as both drives are off resonance by at least $2\chi_{\rm Q}$. For odd qubit parity the cavity state will have one component that is similar in form to α_{00} from the off-resonance drive and one component similar to α_{01} from the nearly on resonance drive.

Given the similar structure of α_{ijkl} in the four-qubit case to α_{ij} of the two-qubit case, it is clear that the errors introduced by $\chi_{\rm Q}$ mismatch in the four-qubit case will be a generalization of those in the two-qubit case. There will be a reduction of measurement contrast due to an increase in the probability of misidentification, which will again be at most second order in the small parameters $\epsilon_i/\chi_{\rm Q}$. The overlap between any two states $|\alpha_{ijkl}\rangle$ corresponding to qubits in the same parity subspace is very similar to Eqs. (C10) and (C11) for the two-qubit case, and as a result, the intrasubspace decoherence during the drive phase will be at most second order in $\epsilon_i/\chi_{\rm Q}$ for odd-parity superpositions and fourth order for even parity. As in the two-qubit case full coherence will be returned to the qubits by perfect cavity reset.

Despite the $\chi_{\rm Q}$ mismatch the two-qubit case exhibits symmetry in α_{ij} within a parity subspace that ensures the detection probabilities are the same for cavity states corresponding to qubit states of the same parity. However, in the four-qubit case this symmetry is no longer present, as in general $\epsilon_2\neq\epsilon_3\neq\epsilon_4$, and as a result, detection probabilities will differ within a parity subspace.

For example, consider an equal superposition of odd-parity states $|a\rangle$ and $|b\rangle$, which after the drive stage are entangled to cavity stages $|\alpha_{a,b}\rangle$, respectively. Detection by the photon counter results in back action on the cavity described by the nonunitary back-action operator $\hat{B}$. Defining the normalized states

$$|\psi_{a,b}\rangle = \frac{\hat{B}|\alpha_{a,b}\rangle}{\langle\alpha_{a,b}|\hat{B}^\dagger\hat{B}|\alpha_{a,b}\rangle} = \frac{\hat{B}|\alpha_{a,b}\rangle}{P_{a,b}}, \tag{C12}$$

where $P_{a,b}$ is the detection probability of the state $|\alpha_{a,b}\rangle$, the resulting state of the cavity-qubit system after detection by the photon counter is

$$|\Psi\rangle = \frac{1}{\sqrt{N}}(\sqrt{P_a}|a\rangle|\psi_a\rangle+\sqrt{P_b}|b\rangle|\psi_b\rangle), \tag{C13}$$

where the normalization factor $N=P_a+P_b$.

The four-qubit states of Eq. (C13) are entangled to distinguishable cavity states such that the reduced four-qubit density matrix's coherence is reduced by the overlap $\langle\psi_b|\psi_a\rangle$. To remove this effect and focus solely on detection probability mismatch we assume that we can perform perfect reset of the cavity and create the state

$$|\Psi\rangle = \frac{1}{\sqrt{N}}(\sqrt{P_a}|a\rangle+\sqrt{P_b}|b\rangle)|0\rangle, \tag{C14}$$

for which the reduced qubit state is the pure state $|\Psi\rangle_{\rm Q}=(\sqrt{P_a}|a\rangle+\sqrt{P_b}|b\rangle)/\sqrt{N}$. Clearly, the output state $|\Psi\rangle_{\rm Q}$ is no longer the input state, and this change is a result of the fact that different detection probabilities for states within the same parity subspace change the basis of measurement of the protocol. To quantify this effect we calculate the magnitude of the overlap between the target state $|\Psi_{\rm T}\rangle_{\rm Q}=(|a\rangle+|b\rangle)/\sqrt{2}$ and the state $|\Psi\rangle_{\rm Q}$, given by

$$O = |\langle\Psi_T|\Psi\rangle_{\rm Q}|^2 = \frac{1}{2}\left(1+\frac{2\sqrt{P_a}\sqrt{P_b}}{P_a+P_b}\right), \tag{C15}$$

which is unity for $P_a=P_b$, as expected.

If we assume the photon counter is a JPM with a subtraction operator back action [38], then the detection probability of the state $|\alpha_i\rangle$ is

$$P_i = 1-\exp\{-|\alpha_i|^2\}. \tag{C16}$$

By Taylor expanding the overlap and discarding terms smaller than $\exp(-2|\alpha_{a/b}|^2)$ we obtain the approximate

overlap

$$O = 1 - \frac{e^{-(|\alpha_a|^2+|\alpha_b|^2)}[\cosh(|\alpha_a|^2 - |\alpha_b|^2) - 1]}{4\left(2 - e^{-|\alpha_a|^2} - e^{-|\alpha_b|^2}\right)} + O\left(e^{-3|\alpha_{a/b}|^2}\right). \quad \text{(C17)}$$

Since we are interested in the effect of detection probability mismatch, we can assume $\alpha_{a,b}$ differ only in magnitude and set $|\alpha_a| = |\alpha|$ and $|\alpha_b| = |\alpha|(1+\delta)$ without loss of generality. The overlap can then be rewritten as

$$O = 1 - \frac{e^{-|\alpha|^2(2+2\delta+\delta^2)}\{\cosh[|\alpha|^2(2\delta+\delta^2)] - 1\}}{4\left(2 - e^{-|\alpha|^2} - e^{-|\alpha|^2(1+\delta)^2}\right)}. \quad \text{(C18)}$$

To examine the scaling of the overlap, we assume that $\delta \ll 1$ and keep only terms up to order δ^2 in the Taylor series, which gives

$$O = 1 - \frac{\delta^2|\alpha|^4 e^{-2|\alpha|^2}}{4\left(1 - e^{-|\alpha|^2}\right)} + O(\delta^3). \quad \text{(C19)}$$

Four-qubit χ_{Q} mismatch causes a difference in the cavity coherent-state amplitude for states in the same parity subspace that scales as $\delta^2 \propto (\epsilon_i^2 - \epsilon_j^2)/\chi_{\mathrm{Q}}^2$. As we assume $\epsilon_i/\chi_{\mathrm{Q}}$ is a small parameter, then $(\epsilon_i^2 - \epsilon_j^2)/\chi_{\mathrm{Q}}^2$ is as small or smaller, so the assumption that $\delta \ll 1$ is valid.

From Eq. (C19) we see that the error in the output state scales as $(\epsilon_i^2 - \epsilon_j^2)/\chi_{\mathrm{Q}}^2$ and is damped by the factor $|\alpha|^4 e^{-2|\alpha|^2}/4$. For $|\alpha| = 3$ as used in the main text this damping factor is on the order of 10^{-6}, so any error in the output state caused by detection probability mismatch is negligible.

A better approximation of the detection probability in the case where the JPM can also relax inelastically is [5]

$$P_i \approx 1 - \exp\left\{-|\alpha_i|^2 \frac{\gamma_{\mathrm{J}}}{\gamma_{\mathrm{J}} + \gamma_{\mathrm{R}}}\right\}. \quad \text{(C20)}$$

Using $\gamma_{\mathrm{J}} = \gamma_{\mathrm{R}}$ as elsewhere, then the error of Eq. (C19) is damped by a factor $\propto|\alpha|^4 e^{-|\alpha|^2}$. For $|\alpha| = 3$ as before, this is on the order of 10^{-2}, which again results in a negligible effect that will only decrease with increasing cavity photon number.

APPENDIX D: QUBIT DECOHERENCE AND CAVITY DECAY

When χ_{Q} mismatch is present, there can be a phase difference between cavity states corresponding to qubit states with the same parity, as discussed for two qubits in Sec. C 1. In this Appendix we examine the effect this has on intrasubspace coherence when a cavity decay mechanism is introduced, as described in the main text.

We start with a typical postdrive or imperfect reset state of the form

$$\hat{\rho}(0) = \sum_{s,s'} c(s,s')|s\rangle\langle s'| \otimes \hat{\rho}_{s,s'}(0) \otimes \hat{\rho}_{\mathrm{B}}, \quad \text{(D1)}$$

where s,s' label the state of the qubits, $\hat{\rho}_{s,s'}(0)$ are the qubit-dependent cavity matrices, and the environmental bath is represented by the state $\hat{\rho}_{\mathrm{B}}$, which is assumed to be stationary and a thermal state. Additionally, we assume that the qubit states have no intrinsic time dependence; that is, we work in the rotating frame of the qubits.

We consider the initial state of the qubits to be an equal superposition of two states in the same parity subspace, which for simplicity we have labeled as $|0\rangle$ and $|1\rangle$. This results in the initial system state

$$\hat{\rho}_{\mathrm{S}}(0) = \tfrac{1}{2}(|0\rangle\langle 0| \otimes |\alpha_0\rangle\langle\alpha_0| + |0\rangle\langle 1| \otimes |\alpha_0\rangle\langle\alpha_1| + |1\rangle\langle 0| \otimes |\alpha_1\rangle\langle\alpha_0| + |1\rangle\langle 1| \otimes |\alpha_1\rangle\langle\alpha_1|), \quad \text{(D2)}$$

where $\hat{\rho}_{s,s'}(0) = |\alpha_s\rangle\langle\alpha_{s'}|$. Due to χ_{Q} mismatch α_0 and α_1 differ in only their phase, and we can set

$$\alpha_0 = |\tilde{\alpha}|e^{i\varphi_0}, \quad \alpha_1 = |\tilde{\alpha}|e^{i\varphi_1}. \quad \text{(D3)}$$

Assuming that the cavity is in a coherent state is accurate for a post-drive-stage state, but the postreset state will be a more general state of the form $\hat{\rho}_{s,s'}(0) = |\psi_s\rangle\langle\psi_{s'}|$. Nevertheless, we are eventually interested in steady-state dynamics, which are independent of the initial state of the cavity (under the Born-Markov approximation). We will treat the post-drive-stage situation first and then generalize to the postreset state.

To solve for $\hat{\rho}_{s,s'}(t)$, we will use the Wigner characteristic function approach. We define the Wigner characteristic function $\chi_{ss'}(\alpha,t)$ of the state $\hat{\rho}_{s,s'}(t)$ as

$$\hat{\rho}_{s,s'}(t) = \frac{1}{\pi}\int d^2\alpha\, \chi_{ss'}(\alpha,t)\hat{D}(-\alpha), \quad \text{(D4)}$$

where $\hat{D}(\beta)$ is the displacement operator.

If we assume a Jaynes-Cumming-type interaction between the cavity and a bosonic environment with smooth spectral density, then following [41], we arrive at the analytic solution for $\chi_{ss'}(\alpha,t)$,

$$\chi_{ss'}(\alpha,t) = \chi_{ss'}(\alpha e^{-t(\kappa - i\omega)},0)e^{[\frac{\eta}{2}|\alpha|^2(e^{-2t\kappa}-1)]}, \quad \text{(D5)}$$

where κ is the decay rate of the cavity, ω is the frequency of the cavity mode, and $\eta = 1 + 2n(\omega)$, with $n(\omega)$ being the Bose distribution at frequency ω.

In order to quantify the absolute maximum amount of decoherence, we are interested in the steady-state solution ($t \to \infty$) of Eq. (D5),

$$\tilde{\chi}_{ss'}(\alpha) = \chi_{ss'}(0,0)e^{-\frac{\eta}{2}|\alpha|^2}. \quad \text{(D6)}$$

Using the facts that

$$\chi_{ss'}(0,0) = \frac{1}{4\pi}\mathrm{Tr}[\hat{\rho}_{s,s'}(0)], \quad \text{(D7)}$$

$$\chi_{10}(\alpha,t) = \bar{\chi}_{01}(-\alpha,t), \quad \text{(D8)}$$

we obtain

$$\tilde{\chi}_{00}(\alpha) = \tilde{\chi}_{11}(\alpha) = \frac{1}{4\pi}e^{-\frac{\eta}{2}|\alpha|^2}, \quad \text{(D9)}$$

$$\tilde{\chi}_{01}(\alpha) = \exp[|\tilde{\alpha}|^2(e^{i(\varphi_1-\varphi_0)} - 1)]\frac{1}{4\pi}e^{-\frac{\eta}{2}|\alpha|^2}, \quad \text{(D10)}$$

$$\tilde{\chi}_{10}(\alpha) = \exp[|\tilde{\alpha}|^2(e^{i(\varphi_0-\varphi_1)} - 1)]\frac{1}{4\pi}e^{-\frac{\eta}{2}|\alpha|^2}. \quad \text{(D11)}$$

Each of Eqs. (D9), (D10), and (D11) can be reduced to $\tilde{\chi}_{ss'}(\alpha) = F_{ss'}(\alpha_0,\alpha_1)\chi_{\mathrm{Thermal}}(\alpha,\omega)$, where $\chi_{\mathrm{Thermal}}(\alpha,\omega) = e^{-\frac{\eta}{2}|\alpha|^2}/4\pi$ is the Wigner characteristic function for a thermal state at frequency ω.

In light of this simplification the steady-state solution for the full system reduces to

$$\hat{\rho}_S = \sum_{s,s'} c(s,s') F_{ss'}(\alpha_0,\alpha_1)|s\rangle\langle s| \otimes \frac{1}{\pi}\int d^2\alpha\, \chi_{\text{Thermal}}(\alpha,\omega)\hat{D}(-\alpha), \tag{D12}$$

where $F_{ss'}(\alpha_s,\alpha_{s'}) = \exp[|\tilde{\alpha}|^2(e^{i(\varphi_s-\varphi_{s'})}-1)]$. As this is a product state, it is trivial to trace out the state of the cavity and obtain the state of the qubits alone,

$$\hat{\rho}_Q = \tfrac{1}{2}(|0\rangle\langle 0| + F_{01}(\alpha_0,\alpha_1)|0\rangle\langle 1| + F_{10}(\alpha_1,\alpha_0)|1\rangle\langle 0| + |1\rangle\langle 1|). \tag{D13}$$

For two qubits, we examine the damping envelope of the off-diagonal elements, given by

$$F_{01}(\alpha_0,\alpha_1) = \exp\left[-|\tilde{\alpha}|^2(e^{2i\varphi_0}+1)\right], \tag{D14}$$

where we have used the fact that $\varphi_0 - \varphi_1 = 2\varphi_0 - \pi$ for two qubits, as can be calculated from either pair of expressions in Eq. (C2). We are interested in the absolute value of this envelope, which is given by

$$|F_{01}(\alpha_0,\alpha_1)| = \exp\left(-|\tilde{\alpha}|^2 \mathrm{Re}\{(e^{2i\varphi_0}+1)\}\right) = \exp\left\{-|\tilde{\alpha}|^2\left[1-\cos\left(\frac{\pi}{\chi_Q}\epsilon\right)\right]\right\}, \tag{D15}$$

where the second equality comes from using Eq. (C2) to define $e^{2i\varphi_0}$. From this we see that the decoherence depends on both the cavity occupation and the magnitude of the χ_Q mismatch, being maximal when $\epsilon/\chi_Q = 1$. Using $|\alpha|^2 = 9$ as used elsewhere and a strong mismatch of $\epsilon/\chi_Q = 0.1$, the qubit coherence is reduced to 64% in the steady state. However, for a high-Q cavity we do not expect any photon loss during the parity readout protocol, and as such, the postreset state is of greater interest.

Generalizing to the postreset state, we need only change the definition of the damping envelope to

$$F_{ss'} = \mathrm{Tr}[\hat{\rho}_{s,s'}(0)] = \langle\psi_{s'}|\psi_s\rangle, \tag{D16}$$

where $|\psi_s\rangle$ is the state after detection and imperfect reset for an initial cavity state $|\alpha_s\rangle$. We will consider the worst-case scenario for the states $|\alpha_{0/1}\rangle$, where the damping envelope of Eq. (D15) reduces to $\exp(-2|\tilde{\alpha}|^2)$. This occurs for $\epsilon = \chi_Q$, where the states $|\alpha_{0/1}\rangle$ lie on the real axis with $\alpha_0 = -\alpha_1$. This is the worst case as the states are maximally distinguishable, and correspondingly, we expect the states $|\psi_{0/1}\rangle$ to also be maximally distinguishable in this case.

Figure 5 shows a numerical simulation of $1 - F_{01}$ for the worst-case postreset state as a function of both the initial cavity occupation $|\tilde{\alpha}|^2$ and the number of photons removed by the photon detector. For these simulations, the detector was assumed to be a JPM with subtraction operator back action [38]. Multiple photons can be removed due to JPM inelastic relaxation. As can be seen, even for the worst-case scenario, qubit coherence is reduced by less than 1%. As we expect $\epsilon \ll \chi_Q$ in a realistic experiment, the decoherence caused by postreset-state photon loss will be far from the upper bound presented here and can be considered inconsequential.

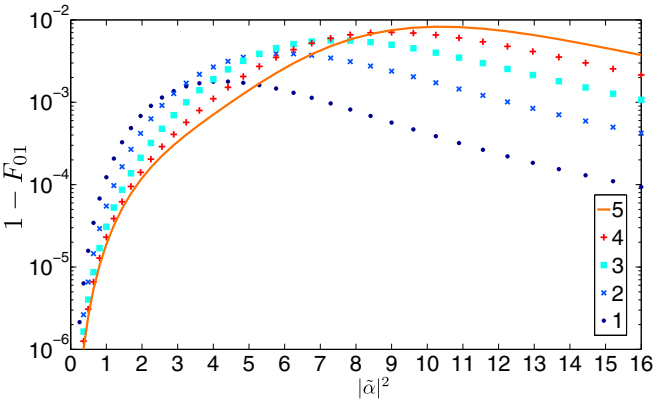

FIG. 5. (Color online) $1 - F_{01}$ as a function of the cavity occupation prior to detection and imperfect reset (horizontal axis) and the number of photons removed from the cavity by the photon detector (color and line style). The initial cavity states considered are maximally distinguishable, so this represents the worst-case scenario.

APPENDIX E: HIGHER-ORDER EFFECTS BEYOND THE DISPERSIVE HAMILTONIAN

While the dispersive Hamiltonian is the first-order approximation to the cavity-qubit coupling in the relevant regime of our protocol, it is worthwhile to consider the effects on the protocol of the full Jaynes-Cummings Hamiltonian for the

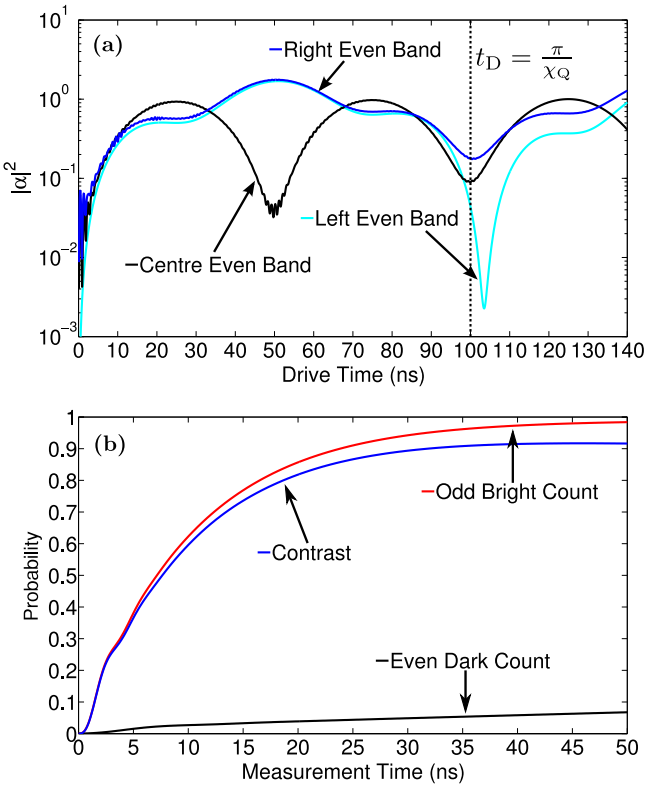

FIG. 6. (Color online) (a) Cavity occupation for even-parity qubit states with Jaynes-Cummings cavity-qubit coupling. (b) Bright- and dark-count rates and measurement contrast for the cavity photon numbers of (a), assuming the even state is from the right band (worst case).

cavity-qubit coupling, given by

$$\hat{H}_{\mathrm{JC}} = \omega_{\mathrm{C}}\hat{a}^{\dagger}\hat{a} - \sum_{k=0}^{N}\frac{1}{2}\omega_{\mathrm{Q}}\hat{\sigma}_{z}^{k} + \sum_{k=0}^{N} g_{k}(\hat{\sigma}_{+}^{k}\hat{a} + \hat{\sigma}_{-}^{k}\hat{a}^{\dagger}), \quad \text{(E1)}$$

where g_k is the cavity-qubit coupling for qubit k. The major effects of the full Jaynes-Cummings Hamiltonian occur during the drive stage.

The first is an asymmetric shift to the cavity frequency within a parity subspace due to the Kerr-like interaction term, which is one order of approximation higher than the dispersive Hamiltonian. The result of this is that the minima of the even-qubit-parity cavity occupation curves no longer coincide, as can be seen in Fig. 6(a) for the four-qubit case. The second major effect is the formation of dressed cavity-qubit states, the result of which is that there is residual cavity occupation for even-parity states, and the minima are no longer zero for all even-parity states. Therefore, for no choice of t_{D} will the cavity be in the vacuum state if the qubits are in an even-parity state. This reduces the measurement contrast, although as can be seen in Fig. 6(b), this reduction is only on the order of a few percent, and measurement contrasts approaching 92% can still be achieved with the same parameters as in the main text.

These effects can be mitigated by increasing the cavity-qubit detuning, in which case the parity measurement contrast asymptotes to the dispersive value. However, this either decreases χ_{Q} and therefore increases the length of the drive stage or necessitates also increasing the cavity-qubit couplings (to keep χ_{Q} constant), which is advisable only to the point where the rotating-wave approximation begins to break down. It is also possible to improve the contrast by better pulse shaping in the drive stage, and this will be the focus of future work. As can also be seen in Fig. 6(a), the fact that the even-qubit-parity cavity photon states are not the same between parity bands would cause intrasubspace qubit decoherence. Full coherence would be returned by perfect reset, unless photon loss occurs (either through a detection or other mechanism). However, photon loss of any kind is so unlikely for these low-occupation cavity states that the effect on qubit coherence is minimal, on the order of a few percent at most.

[1] A. Blais, R.-S. Huang, A. Wallraff, S. M. Girvin, and R. J. Schoelkopf, Phys. Rev. A **69**, 062320 (2004).

[2] J. Gambetta, W. A. Braff, A. Wallraff, S. M. Girvin, and R. J. Schoelkopf, Phys. Rev. A **76**, 012325 (2007).

[3] E. Jeffrey, D. Sank, J. Y. Mutus, T. C. White, J. Kelly, R. Barends, Y. Chen, Z. Chen, B. Chiaro, A. Dunsworth *et al.*, Phys. Rev. Lett. **112**, 190504 (2014).

[4] R. Vijay, D. H. Slichter, and I. Siddiqi, Phys. Rev. Lett. **106**, 110502 (2011).

[5] L. C. G. Govia, E. J. Pritchett, C. Xu, B. L. T. Plourde, M. G. Vavilov, F. K. Wilhelm, and R. McDermott, Phys. Rev. A **90**, 062307 (2014).

[6] M. Nielsen and I. Chuang, *Quantum Computation and Quantum Information* (Cambridge University Press, Cambridge, 2000).

[7] A. G. Fowler, M. Mariantoni, J. M. Martinis, and A. N. Cleland, Phys. Rev. A **86**, 032324 (2012).

[8] A. Peruzzo, J. McClean, P. Shadbolt, M.-H. Yung, X.-Q. Zhou, P. J. Love, A. Aspuru-Guzik, and J. L. O'Brien, Nat. Commun. **5**, 4213 (2014).

[9] D. Gottesman and I. L. Chuang, Nature (London) **402**, 390 (1999).

[10] C. W. J. Beenakker, D. P. DiVincenzo, C. Emary, and M. Kindermann, Phys. Rev. Lett. **93**, 020501 (2004).

[11] C. L. Hutchison, J. M. Gambetta, A. Blais, and F. K. Wilhelm, Can. J. Phys. **87**, 225 (2009).

[12] D. Ristè, M. Dukalski, C. A. Watson, G. de Lange, M. J. Tiggelman, Y. M. Blanter, K. W. Lehnert, R. N. Schouten, and L. DiCarlo, Nature (London) **502**, 350 (2013).

[13] R. Ruskov and A. N. Korotkov, Phys. Rev. B **67**, 241305 (2003).

[14] S. E. Nigg and S. M. Girvin, Phys. Rev. Lett. **110**, 243604 (2013).

[15] J. M. Chow, J. M. Gambetta, E. Magesan, D. W. Abraham, A. W. Cross, B. R. Johnson, N. A. Masluk, C. A. Ryan, J. A. Smolin, S. J. Srinivasan *et al.*, Nat. Commun. **5**, 4015 (2014).

[16] L. Steffen, Y. Salathe, M. Oppliger, P. Kurpiers, M. Baur, C. Lang, C. Eichler, G. Puebla-Hellmann, A. Fedorov, and A. Wallraff, Nature (London) **500**, 319 (2013).

[17] B. Vlastakis, G. Kirchmair, Z. Leghtas, S. E. Nigg, L. Frunzio, S. M. Girvin, M. Mirrahimi, M. H. Devoret, and R. J. Schoelkopf, Science **342**, 607 (2013).

[18] D. P. DiVincenzo and F. Solgun, New J. Phys. **15**, 075001 (2013).

[19] L. Tornberg, S. Barzanjeh, and D. P. DiVincenzo, Phys. Rev. A **89**, 032314 (2014).

[20] M. Devoret and R. Schoelkopf, Science **339**, 1169 (2013).

[21] F. Mallet, F. R. Ong, A. Palacios-Laloy, F. Nguyen, P. Bertet, D. Vion, and D. Esteve, Nat. Phys. **5**, 791 (2009).

[22] Y.-F. Chen, D. Hover, S. Sendelbach, L. Maurer, S. T. Merkel, E. J. Pritchett, F. K. Wilhelm, and R. McDermott, Phys. Rev. Lett. **107**, 217401 (2011).

[23] Y. Kubo, F. R. Ong, P. Bertet, D. Vion, V. Jacques, D. Zheng, A. Dréau, J.-F. Roch, A. Auffeves, F. Jelezko *et al.*, Phys. Rev. Lett. **105**, 140502 (2010).

[24] J. D. Pritchard, J. A. Isaacs, M. A. Beck, R. McDermott, and M. Saffman, Phys. Rev. A **89**, 010301 (2014).

[25] S. D. Hogan, J. A. Agner, F. Merkt, T. Thiele, S. Filipp, and A. Wallraff, Phys. Rev. Lett. **108**, 063004 (2012).

[26] T. Frey, P. J. Leek, M. Beck, A. Blais, T. Ihn, K. Ensslin, and A. Wallraff, Phys. Rev. Lett. **108**, 046807 (2012).

[27] R. Miller, T. E. Northup, K. M. Birnbaum, A. Boca, A. D. Boozer, and H. J. Kimble, J. Phys. B **38**, S551 (2005).

[28] J. Miguel-Sánchez, A. Reinhard, E. Togan, T. Volz, A. Imamoglu, B. Besga, J. Reichel, and J. Estève, New J. Phys. **15**, 045002 (2013).

[29] Y. Chen, D. Sank, P. O'Malley, T. White, R. Barends, B. Chiaro, J. Kelly, E. Lucero, M. Mariantoni, A. Megrant *et al.*, Appl. Phys. Lett. **101**, 182601 (2012).

[30] J. Kelly, R. Barends, A. G. Fowler, A. Megrant, E. Jeffrey, T. C. White, D. Sank, J. Y. Mutus, B. Campbell, Y. Chen *et al.*, Nature (London) **519**, 66 (2015).

[31] L. C. G. Govia, E. J. Pritchett, S. T. Merkel, D. Pineau, and F. K. Wilhelm, Phys. Rev. A **86**, 032311 (2012).

[32] A. Poudel, R. McDermott, and M. G. Vavilov, Phys. Rev. B **86**, 174506 (2012).

[33] G. Ribeill, I. Pechenezhski, T. Thorbeck, C. Howington, M. Hutchings, L. Govia, F. Wilhelm, B. Plourde, and R. McDermott, Bull. Am. Phys. Soc. **60** (2015), http://meetings.aps.org/link/BAPS.2015.MAR.G39.5.

[34] M. Dakna, T. Anhut, T. Opatrný, L. Knöll, and D.-G. Welsch, Phys. Rev. A **55**, 3184 (1997).

[35] D. K. L. Oi, V. Potoček, and J. Jeffers, Phys. Rev. Lett. **110**, 210504 (2013).

[36] F. Boitier, J.-B. Dherbecourt, A. Godard, and E. Rosencher, Appl. Phys. Lett. **94**, 081112 (2009).

[37] To our knowledge the imbalanced thresholds between gates and measurement have not been explored in detail in the fault-tolerance literature.

[38] L. C. G. Govia, E. J. Pritchett, and F. K. Wilhelm, New J. Phys. **16**, 045011 (2014).

[39] W. Magnus, Commun. Pure Appl. Math. **7**, 649 (1954).

[40] B. Peropadre, G. Romero, G. Johansson, C. M. Wilson, E. Solano, and J. J. García-Ripoll, Phys. Rev. A **84**, 063834 (2011).

[41] I. Serban, B. L. T. Plourde, and F. K. Wilhelm, Phys. Rev. B **78**, 054507 (2008).